Influence of ZnO nanowire array morphology on field emission characteristics

S. Garry*, É. McCarthy, J.P. Mosnier, E. McGlynn*

School of Physical Sciences, National Centre for Plasma Science & Technology, Dublin City University, Glasnevin, Dublin 9, Ireland.

Authors to whom correspondence should be addressed: seamus.garry2@mail.dcu.ie, enda.mcglynn@dcu.ie.

Abstract

In this work the growth and field emission properties of vertically aligned and spatially ordered and unordered ZnO nanowires are studied. Spatially ordered nanowire arrays of controlled array density are synthesised by both chemical bath deposition and vapour phase transport using an inverse nanosphere lithography technique, while spatially unordered arrays are synthesised by vapour phase transport without lithography. The field emission characteristics of arrays with 0.5 µm, 1.0 µm, and 1.5 µm inter-wire distances, as well as unordered arrays, are examined, revealing that with the range of values examined field emission properties are mainly determined by variations in nanowire height, and show no correlation with nanowire array density. Related to this, we find that a significant variation in nanowire height in an array also leads to a reduction in catastrophic damage observed on samples during field emission because arrays with highly uniform heights are found to suffer significant arcing damage. We discuss these results in light of recent computational studies of comparable nanostructure arrays and find strong qualitative agreement between our results and the computational predictions. Hence the results presented in this work should be useful in informing the design of ZnO nanowire arrays in order to optimise their field emission characteristics generally.

Introduction

There is strong ongoing interest in the use of ZnO nanostructure arrays for device applications in optoelectronics [1, 2], photo-voltaics [3], gas sensing [4], catalysis [5], and piezo-electric energy generation [6] for example. In particular applications requiring unipolar

carrier operation avoid the well-known p-type doping difficulty in ZnO. Amongst these application areas, one of particular interest is the field of vacuum microelectronics based on the process of electron field emission (FE), which can be used for devices such as flat panel displays [7] or micro x-ray sources [8]. ZnO may be grown in a variety of possible nanostructure morphologies which makes it a useful material for the study of FE and, in particular, the study of the impact of nanowire morphology on electron emission and the search for optimum nanostructure morphologies. A large number of these studies rely on the use of "bottom-up" methods for nanostructure synthesis, similar to the case of other nanostructured materials, and thus such nanostructures naturally display variations in density, ordering, height etc.

Array density has been proposed to have a significant impact on the efficiency and uniformity of FE devices [9-12]. Control of array density may be achieved using nanosphere lithography (NSL) and there are many examples in the literature of well ordered, periodic arrays of ZnO nanowires grown using NSL [1,13-16]. NSL relies on producing a lithographic mask comprised of a close packed monolayer of e.g. polystyrene beads which can be produced with differing aperture sizes and separation. It is often preferable to other patterning techniques such as e-beam lithography and mask lithography due to its low cost and the ability to easily pattern large areas. However, systematic studies of the effects on the efficiency and uniformity of FE devices of array density, nanowire distribution periodicity/uniformity, and especially non-uniformity/randomness in these quantities, in addition to nanowire height non-uniformity/randomness, are very rare in the literature and we know of no examples for the specific case of ZnO nanowires. Amongst the most significant work in this underexplored field is a very recent publication by Dall'Agnol and den Engelsen [17] which reports a computational study of these effects introduced in the context of carbon nanotube arrays, but more broadly applicable to ZnO and other material system nanowire arrays.

In this work, we report the use of a catalyst-free inverse NSL masking technique, allowing us to produce ZnO nanowire arrays without the difficulties associated with the use of metallic catalyst material, in particular the presence of metal nanowire tips, which may influence FE properties in an manner hard to determine. The use of an inverse NSL technique allows both low temperature deposition techniques such as chemical bath deposition (CBD) and high temperature techniques such as vapour phase transport (VPT), allowing a broader range of nanowire morphologies to be examined. We present results on the growth, characterisation and FE studies of ZnO nanowire arrays grown using both VPT and CBD

techniques. These arrays were produced with controlled inter-wire spacings of 0.5 µm, 1.0 µm, and 1.5 µm in addition to two samples grown by VPT without controlled density. A total of ten ZnO nanowire arrays are examined. We comment on relevant aspects of nanowire morphology and how these are likely to influence FE behaviour and we compare our experimental results with the predictions of the most recent computational studies [17], finding excellent qualitative agreement in terms of the key aspects of morphology which determine FE behaviour. Based on this consistency between experimental and computational results we are confident that the results presented here will be valuable in informing the design of ZnO nanowire arrays in order to optimise their FE behaviour.

Methods

Sample preparation

Silicon substrates with (100) orientation were coated with a ZnO buffer layer using a method combining drop coating and CBD [18, 19] to provide suitable nucleation sires for ZnO nanowire growth and to ensure that such growth is c-axis aligned.

In order to deposit nanowire arrays with controlled array density, ZnO buffer layers are then coated with a patterned ordered silica template produced by nanosphere lithography [20]. ZnO buffer layers were coated with a self-assembled monolayer of polystyrene nanospheres, using a water transfer method [16] and allowed to dry. An acid-catalysed silica sol, prepared using of 0.5 ml of tetraethyl orthosilicate and 0.5 ml of hydrochloric acid in 20 ml of ethanol was deposited into the interstitial spaces left exposed by the close-packed nanosphere pattern. The nanospheres are then removed by ultrasonication in toluene and the remaining silica template is densified by being annealed at 550 °C with a 15 °C/min ramp rate. This results in a silica layer covering the substrate with a periodic array of apertures where the ZnO buffer layer is exposed (the sole locations where ZnO nanowires will subsequently grow) only where the nanospheres originally made contact with the buffer layer and masked it during the sol deposition.

ZnO nanowires were deposited using two techniques, CBD and VPT [21, 22], with nanospheres of 0.5, 1.0, and 1.5 µm diameter. CBD depositions were carried out using a 25 mM zinc acetate solution in DI-H_2O at 60 - 70°C for 90 mins. VPT depositions were carried out in a single zone tube furnace, using equal masses of graphite and ZnO (60 mg) as the source materials. The furnace was heated to 800 °C for 10 mins and then ramped to 900 °C at a rate of

10 °C/min. The total growth time is 1 hour after which the furnace is allowed to cool to room temperature.

A more detailed description of sample preparation is provided in the supporting information.

Characterisation

Nanowire morphology and crystal structure were examined using scanning electron microscopy (SEM; Karl-Zeiss EVO series). Field emission properties were examined in a home-made system using a parallel-plate electrode configuration in a vacuum chamber with a base pressure of ~10^{-8} mbar [23]. A circular stainless steel anode of 8 mm diameter is used, and the sample was positioned at a fixed distance of (250 ± 10) µm from the anode. The electrode assembly is mounted in series with a current-limiting resistance of ~231 kΩ. The voltage is swept between 50 V and 2500 V in steps of 1 V using a high voltage source (Stanford PS350). The current at each step is measured using a picoammeter (Keithley 6485). In all cases the initial I-V measurements taken exhibit hysteresis, as has been reported previously in the literature [24-26]. This hysteresis disappears after adequate conditioning of the sample, which is carried out by repeating I-V measurements in a cyclical manner. Typically hysteresis is no longer observed after ~150 conditioning cycles.

Results and Discussion

Figure 1 shows SEM images of ZnO nanowire arrays produced using the CBD technique. A feature of arrays produced in this way is extreme uniformity in nanowire height, which may be controlled reliably by altering the growth time. As can be seen in figure 1, CBD nanowire arrays exhibit excellent uniformity in array density as growth does not occur on those areas masked with silica.

In contrast to nanowires deposited by CBD, those deposited using VPT are typically longer and tend to have more tapered tips. In general, VPT nanowire arrays tend to have large variations of nanowire height, even between adjacent nanowires, however this is reduced in the case of arrays produced using an NSL silica mask [19]. Figure 2 presents the samples produced using VPT in this work, parts (a) & (b), show arrays where no attempt was made to control density while parts (c) – (g) present samples grown using the NSL silica mask technique.

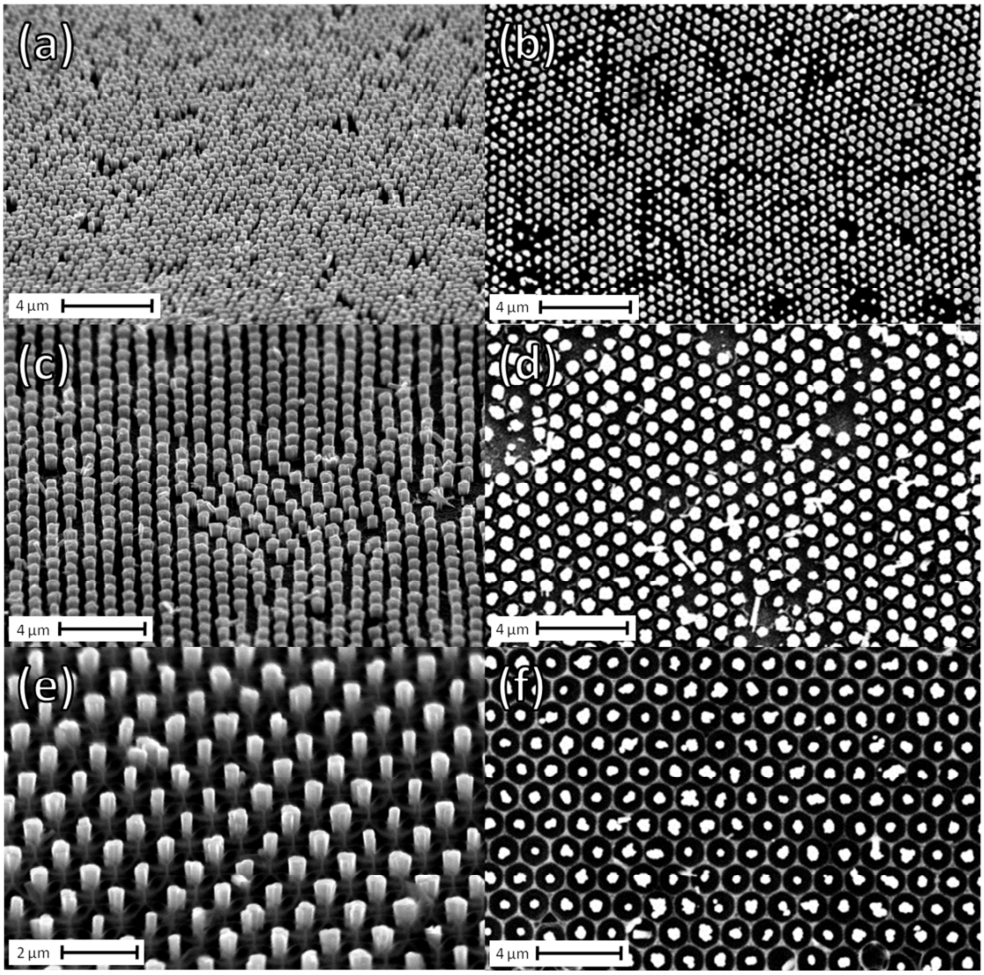

Figure 1: SEM images of CBD produced ZnO nanowire arrays. Parts a) and b) show an array with 0.5 µm interwire spacing (average height: 0.417 µm) at a tilt of 45° and 0° respectively. Similarly, parts c) and d) show 1.0 µm (average height: 0.541 µm) and e) and f) show 1.5 µm (average height: 0.683 µm) interwire spacing arrays.

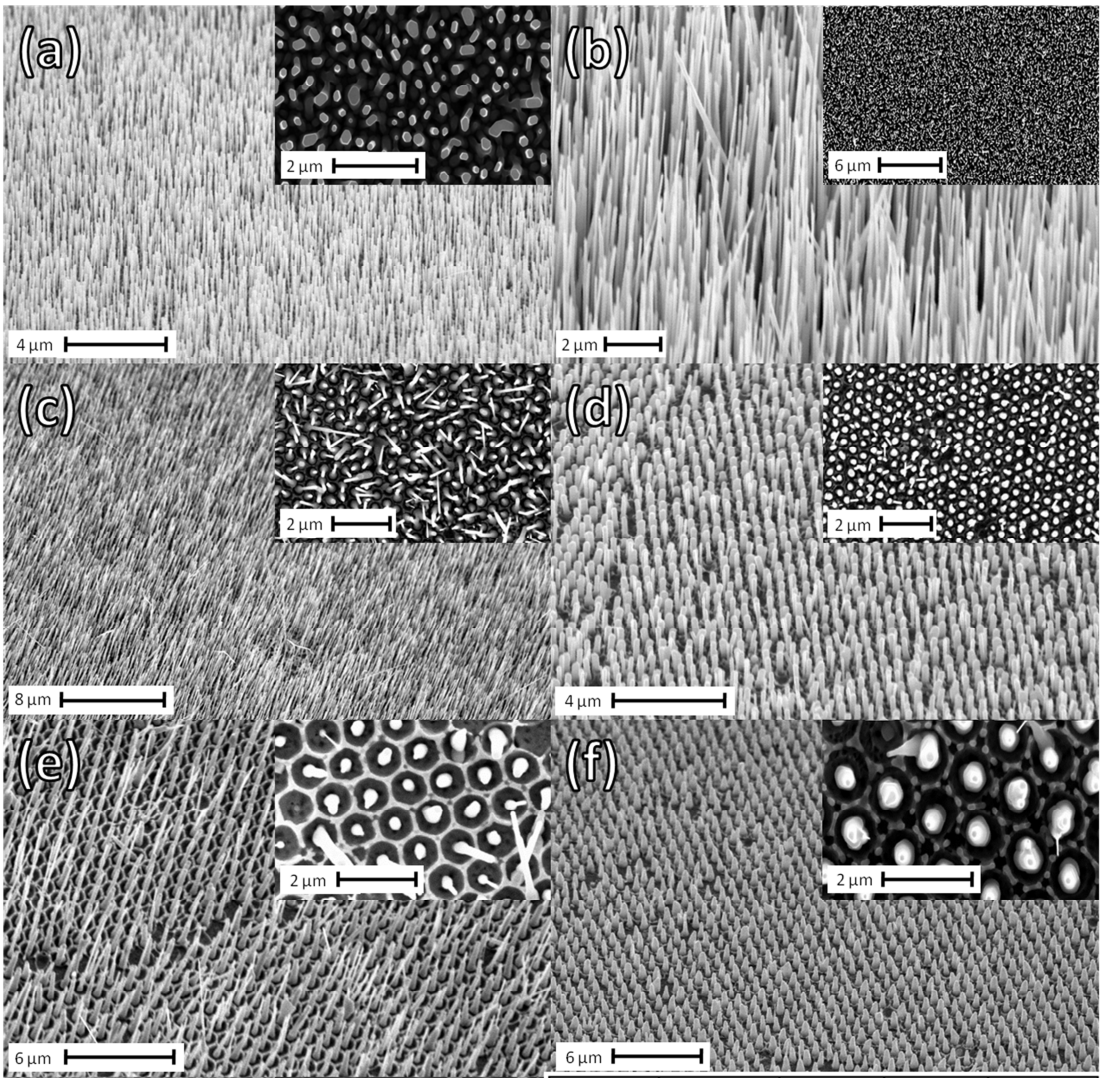

Sample Type	Spacing (µm)	Avg. Height (µm)	Standard Deviation	Arcing Damage
CBD	0.5	0.417	0.056	Y
	1.0	0.541	0.058	Y
	1.5	0.683	0.060	Y
VPT	Uncontrolled	1.383	0.213	N
	Uncontrolled	6.982	1.767	N
	0.5	4.702	0.852	N
	0.5	0.797	0.109	Y
	1.0	3.136	0.749	N
	1.0	1.449	0.123	Y
	1.5	1.658	0.325	N

Figure 2: SEM images of ZnO nanowire arrays grown by VPT. Parts a) and b) show arrays where array density was not controlled (with average nanowire heights of 1.383 and 6.982 µm, respectively); c) and d) show arrays with 0.5 µm spacing (average heights of 4.702 µm and 0.797 µm, respectively); e) and f) show arrays with 1.0 µm spacing (average heights of 3.136 µm and 1.449 µm, respectively); g) shows a 1.5 µm spaced array (average height: 1.658 µm); h) table showing average nanowire height, standard deviation in height, and whether catastrophic arcing damage occurred during FE.

Field emission

All samples examined exhibited some changes in morphology post-FE, however the majority of these changes are limited to minor melting of nanowire tips, with some small areas where nanowires are entirely melted. These are present on only small areas of each sample and are not believed to significantly affect FE performance. Examples of these areas are presented in the accompanying supporting information.

On some samples however, more significant damage was observed. Structural disruption of the substrate such that nanowires, buffer layer, and Si substrate apparently 'exploded' over the surrounding area. Figure 3 presents an example of such damage, which typically exhibit conical structures consisting of Si material (based on energy dispersive x-ray measurements in the SEM system) which has been melted due to the high current density during an arcing event (as discussed further in the supporting information). This extreme damage was observed on all 3 CBD samples examined and on 2 (of 7) VPT samples. We note that that there was no observable FE from bare Si substrates or ZnO wafers at our limit of instrumental sensitivity. Furthermore the explosive damage is always at the Si/ZnO interface (and this is also seen for ZrN and ZrC deposits on Si, data not shown). We also note that the silver paste/Si wafer electrical contact at the backside of the sample always remains intact, supporting our explanation of the catastrophic damage as arising from arcing.

FE data from samples exhibiting arcing damage such as shown in figure 3 was not used for further analysis since the impact of such damaged regions on the FE performance is not understood (discussed in greater detail in the supporting information). However, the nature of samples so affected provides very important and useful information about the morphology dependence of FE processes in such nanowire arrays. These samples tended to have significantly more uniform nanowire height than undamaged arrays. These samples correspond to all of those shown in figure 1 and to those shown in parts d) and f) of figure 2. As can be seen from these images, these arrays are extremely uniform, particularly in terms of nanowire height, whereas those samples unaffected by this type of damage tended to have a greater variance in height as shown in part h) of figure 2, where the standard deviation for nanowire height for all samples is presented. In those samples where array density is controlled, a large standard deviation in height appears to have a protective effect against extreme melting damage.

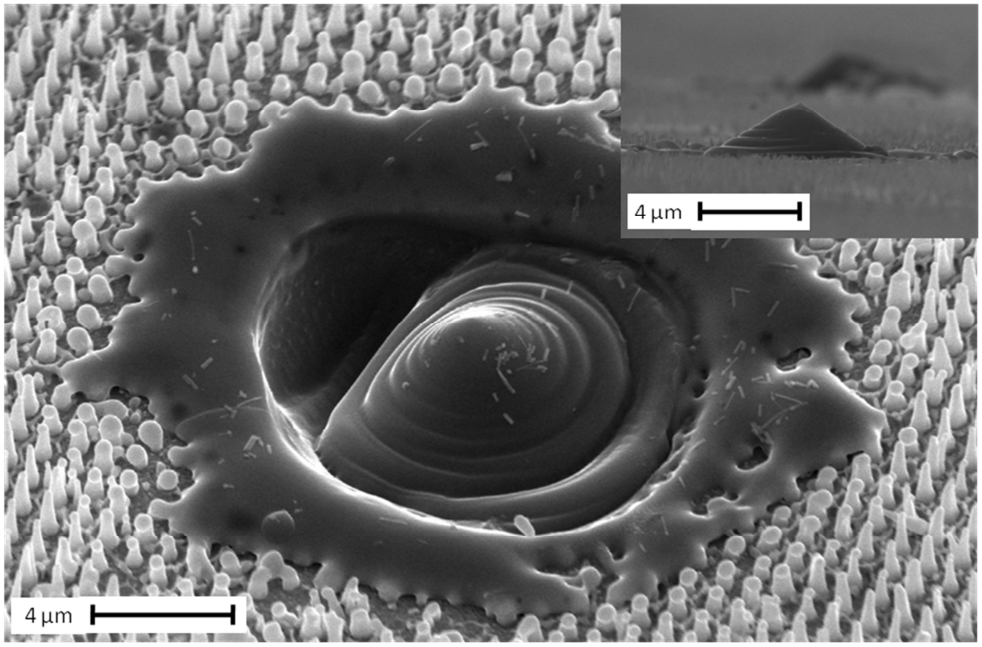

Figure 3: Example of a substrate disruption observed on a number of samples post-FE. Nanowires, buffer layer, and underlying substrate are severely disrupted. An image of one such disruption taken at 90° is shown in the inset and it may be sent that the conical structures are significantly taller than the surrounding nanowires.

A possible explanation is that in the case of arrays with extreme uniformity in nanowire height, a defect in a localised region, such as a precipitate or a slightly taller nanowire, results in a single site that emits at a lower voltage and thus draws a significant fraction of the total current, and is thus likely to melt sooner than its surrounding (mostly non-emitting) nanowires, resulting in a runaway effect as described by Spindt *et al.* [27]. This catastrophic damage was not observed on samples where spacing was not controlled, and again we propose that this is due to the lack of height uniformity for those samples, as shown in the table in figure 2(h). We discuss these hypotheses further below in the context of recent computational predictions for the effects of randomness in nanowire array parameters.

Analysis of FE data (presented in figure 4) is carried out as described in McCarthy *et al.* [23]. All experimental data above the turn-on voltage are converted to a Fowler-Nordheim (FN) plot by plotting $\log_{10}(I/V^2)$ vs 1/V. The slope, m, of the FN plot may be written as:

$$m = -2.97\times10^{9}\,\frac{\phi^{3/2}s(y)}{\beta}$$

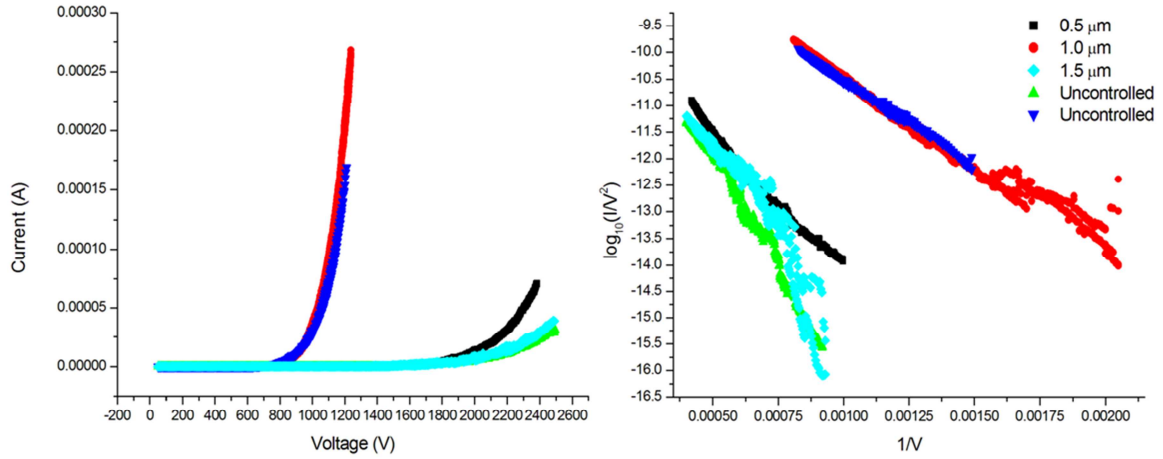

Figure 4: FE data gathered from during FE. Part a) shows I-V curves and part b) shows FN plots over the voltage range where FE is the dominant emission type.

where β is a geometric factor relating the potential difference to the local field at the emitter surface and is dependent on the nanowire array morphology, and s(y) is a function representing the Schottky lowering of the work function barrier; calculation of s(y) is also described in Ref [23]. The field enhancement factor, γ, is a dimensionless quantity which takes both the morphology of the nanowire array and the distance between the anode and sample into account. It is given by $\gamma = \beta \times d$, where d is the anode/sample separation.

Figure 5 shows a plot of the field enhancement factor extracted from the FE data plotted against the array density (the number of nanowires per μm^2) for the remaining five samples. The density for NSL samples is calculated from the diameter of nanosphere used, while the density for unspaced VPT samples is an average value calculated by counting over sample areas of ~ 50 μm^2.

There is no clear trend which relates the array density to indicators of FE performance such as the field enhancement factor. It is likely that other differences in morphology are responsible for such variations, such as nanowire height, details of nanowire faceting and tip area for example. This leads to the conclusion that while nanowire array density may be a significant factor in determining FE properties of similar samples, it cannot be used effectively to compare morphologically dissimilar arrays. For this reason, an approach which includes other morphological factors such as nanowire height, details of nanowire faceting and tip area must also be considered.

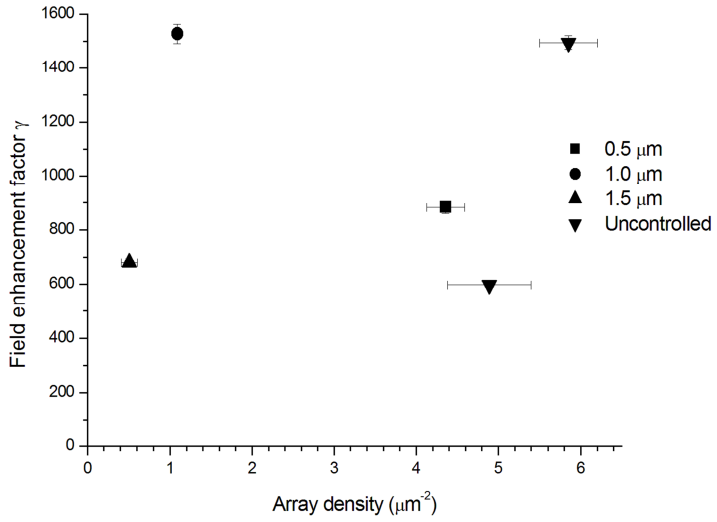

Figure 5: Graph of field enhancement factor γ against array density.

These results run counter to various reports in the literature which assume or conclude that lower nanowire density alone leads to enhanced FE characteristics due to a reduction in the incidence of closely adjacent nanowires "shielding" each other (thus effectively reducing the high aspect ratio advantages such as a larger field enhancement factor expected from such structures) [9-11, 28-30]. However the data from samples examined in this work shows no correlation between array density or spacing/periodicity and field emission performance. It is thus much more likely that the exact FE characteristics are determined by other factors such as variations in nanowire height, details of nanowire faceting and tip area some of which were not controlled in this work.

However, the recent computational work carried out by Dall'Agnol and den Engelsen [17], where the effects of randomising the nanowire height, radius (assuming circular cross-sections), and array density on FE properties of nanotube arrays (of a structure suitable for comparison with our experimental data) are examined, shows that FE performance is much more sensitive to changes in nanowire height in certain regimes of aspect ratio. For example, more than one order of magnitude increase in FE current is predicted from close packed nanowire arrays with random heights where the nanowire spacings are less than the average nanowire height (as is the case for our VPT nanowire morphologies), compared to uniform height arrays. Much smaller increases are predicted for randomisation of the other array parameters (i.e. nanowire radius and array density). These results are in very good agreement with our results above. Firstly they support the hypothesis that the catastrophically damaged

regions observed in the case of arrays with extreme uniformity in nanowire height are due to defects in a localised region, such as a precipitate or a slightly taller nanowire, resulting in a single site that emits at a lower voltage and thus draws a very high (and destructive) local current, with few or none of the other nanowires in the array emitting. By contrast, the samples which did not show this catastrophic damage all have larger standard deviations in height and the emission current is likely to be both enhanced and (due to the random nature of the height variations) more uniformly distributed across the sample, preventing such catastrophic damage due to very large local current densities.

Further empirical evidence, based on our data, for the strong sensitivity of the FE characteristics to the degree of height uniformity is shown in figure 6 which shows a plot of the field enhancement factor extracted from the data in figure 4 plotted against the standard deviation in nanowire height for each sample measured. While the correlation is not perfect, the plot does show a general trend of increasing γ values for samples with a greater standard deviation in height. These results provide some indication that the extracted γ value from such FE measurements on nanowire arrays may be more closely related to the standard deviation in the height of nanowires in the array (i.e. an ensemble property of the array) rather than to the geometrical properties of individual nanowires, as is the case for single or well-spaced emitters, and which is often also assumed to be the case for nanowire arrays [31, 32].

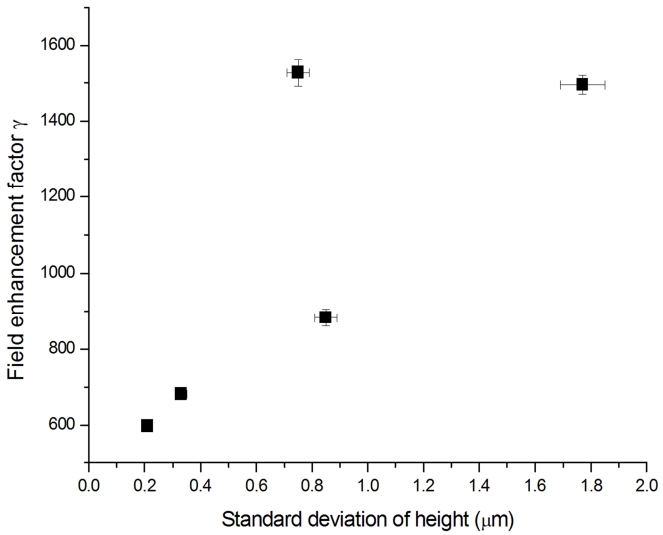

Figure 6*: Graph of field enhancement factor γ vs. standard deviation of nanowire array height.*

Conclusions

We have examined the FE properties of vertically aligned and spatially ordered ZnO nanowire array samples produced using both CBD and VPT techniques. It was found that nanowire array morphology plays a large role in determining FE properties. In almost all cases, the samples under investigation were observed to show some melting during field emission, but there is no indication in most cases that this is detrimental to the overall FE properties of a given sample. In the case of samples showing the smallest variations in nanowire heights, significant catastrophic damage was caused during the FE measurements. Regions of the sample were covered with crater-like marks which in most cases are occupied by a central conical Si structure. Due to concerns about the quality of subsequent I-V data produced by these samples, they were not examined further by FE measurements. This result is explained for the case of arrays with extreme uniformity in nanowire height in terms of localised defects, such as a precipitate or a slightly taller nanowire, resulting in a single (or a small number of) emitting site(s) with significant local current resulting in a runaway destructive process.

The five remaining samples which did not show this catastrophic damage all have larger standard deviations in height and the emission current is thus likely to be both enhanced and more uniformly distributed across the sample. These samples revealed no obvious correlations in either the turn on voltages or field enhancement factors γ with the array inter-wire spacing, as is often expected/assumed. However, when γ is plotted against the standard deviation of nanowire height, we see a suggestive trend whereby FE performance improves when there is greater variation in height. These data indicate that the extracted field enhancement (γ) values from such FE measurements on nanowire arrays may be more closely related to the standard deviation in the height of nanowires in the array (i.e. an ensemble property of the array) rather than to the properties of individual nanowires.

These results are all consistent with the results and predictions recently reported in reference [17] where it is shown that for the three main generic morphological variables in an emitter array (height, radius, separation), randomisation of nanowire radius and separation have only a slight effect on FE performance whereas randomisation of nanowire height has a significantly greater impact on FE emission performance, often orders of magnitude greater.

Based on this strong agreement between experimental and computational results we are confident that the results presented here will be valuable in informing the design of ZnO nanowire arrays in order to optimise their FE behaviour.

Acknowledgements

The authors acknowledge the main financial support of Science Foundation Ireland (SFI) under grant 08-RFPMTR1401. We also acknowledge SFI equipment funding under Grant No. 03/IN3/1361/EC07.

References

1. Wang, X., C.J. Summers, and Z.L. Wang, *Large-Scale Hexagonal-Patterned Growth of Aligned ZnO Nanorods for Nano-optoelectronics and Nanosensor Arrays.* Nano Letters, 2004. **4**(3): p. 423-426.
2. Huang, M.H., et al., *Room-Temperature Ultraviolet Nanowire Nanolasers.* Science, 2001. **292**(5523): p. 1897-1899.
3. Law, M., et al., *Nanowire dye-sensitized solar cells.* Nat Mater, 2005. **4**(6): p. 455-459.
4. Nanto, H., T. Minami, and S. Takata, *Zinc-oxide thin-film ammonia gas sensors with high sensitivity and excellent selectivity.* Journal of Applied Physics, 1986. **60**(2): p. 482-484.
5. Iwasa, N., et al., *Steam reforming of methanol over Pd/ZnO: Effect of the formation of PdZn alloys upon the reaction.* Applied Catalysis A: General, 1995. **125**(1): p. 145-157.
6. Wang, Z.L. and J. Song, *Piezoelectric Nanogenerators Based on Zinc Oxide Nanowire Arrays.* Science, 2006. **312**(5771): p. 242-246.
7. Choi, W.B., et al., *Fully sealed, high-brightness carbon-nanotube field-emission display.* Applied Physics Letters, 1999. **75**(20): p. 3129-3131.
8. Liu, Z., et al., *Carbon nanotube based microfocus field emission x-ray source for microcomputed tomography.* Applied Physics Letters, 2006. **89**(10): p. 103111-3.
9. Rajendra Kumar, R.T., et al., *Control of ZnO nanorod array density by Zn supersaturation variation and effects on field emission.* Nanotechnology, 2007. **18**(21).
10. Patra, S.K. and G.M. Rao, *Field emission current saturation of aligned carbon nanotube---Effect of density and aspect ratio.* Journal of Applied Physics, 2006. **100**(2): p. 024319-5.
11. Suh, J.S., et al., *Study of the field-screening effect of highly ordered carbon nanotube arrays.* Applied Physics Letters, 2002. **80**(13): p. 2392-2394.
12. Read, F.H. and N.J. Bowring, *Field enhancement factors of random arrays of carbon nanotubes.* Nuclear Instruments and Methods in Physics Research Section A: Accelerators, Spectrometers, Detectors and Associated Equipment, 2004. **519**(1–2): p. 305-314.
13. Zhang, X., et al., *Synthesis of large-scale periodic ZnO nanorod arrays and its blue-shift of UV luminescence.* Journal of Materials Chemistry, 2009. **19**(7): p. 962-969.
14. Liu, D.F., et al., *Periodic ZnO nanorod arrays defined by polystyrene microsphere self-assembled monolayers.* Nano Letters, 2006. **6**(10): p. 2375-2378.
15. Fan, H.J., et al., *Arrays of vertically aligned and hexagonally arranged ZnO nanowires: A new template-directed approach.* Nanotechnology, 2005. **16**(6): p. 913-917.
16. Rybczynski, J., et al., *Formation of super arrays of periodic nanoparticles and aligned ZnO nanorods - Simulation and experiments.* Nano Letters, 2004. **4**(10): p. 2037-2040.
17. Dall'Agnol, F. and D. den Engelsen, *Field emission from non-uniform carbon nanotube arrays.* Nanoscale Research Letters, 2013. **8**(1): p. 319.
18. Greene, L.E., et al., *General route to vertical ZnO nanowire arrays using textured ZnO seeds.* Nano Letters, 2005. **5**(7): p. 1231-1236.
19. Byrne, D., et al., *A catalyst-free and facile route to periodically ordered and c-axis aligned ZnO nanorod arrays on diverse substrates.* Nanoscale, 2011. **3**(4): p. 1675-1682.

20. Byrne, D., et al., *A novel, substrate independent three-step process for the growth of uniform ZnO nanorod arrays.* Thin Solid Films, 2010. **518**(16): p. 4489-4492.
21. Kumar, R.T.R., et al., *Growth of ZnO nanostructures on Au-coated Si: Influence of growth temperature on growth mechanism and morphology.* Journal of Applied Physics, 2008. **104**(8): p. 084309-11.
22. Biswas, M., E. McGlynn, and M.O. Henry, *Carbothermal reduction growth of ZnO nanostructures on sapphire—comparisons between graphite and activated charcoal powders.* Microelectronics Journal, 2009. **40**(2): p. 259-261.
23. McCarthy, E., et al., *Field emission in ordered arrays of ZnO nanowires prepared by nanosphere lithography and extended Fowler-Nordheim analyses.* Journal of Applied Physics, 2011. **110**(12): p. 124324-124324.
24. Zhang, H.Z., R.M. Wang, and Y.W. Zhu, *Effect of adsorbates on field-electron emission from ZnO nanoneedle arrays.* Journal of Applied Physics, 2004. **96**(1): p. 624-628.
25. Jacobi, K., G. Zwicker, and A. Gutmann, *Work function, electron affinity and band bending of zinc oxide surfaces.* Surface Science, 1984. **141**(1): p. 109-125.
26. Marien, J., *Field emission study of the specificity of zinc oxide polar surfaces (0001) and (0001). Work function and hydrogen adsorption.* physica status solidi (a), 1976. **38**(2): p. 513-522.
27. Spindt, C.A., et al., *Physical properties of thin-film field emission cathodes with molybdenum cones.* Journal of Applied Physics, 1976. **47**(12): p. 5248-5263.
28. Jo, S.H., et al., *Field-emission studies on thin films of zinc oxide nanowires.* Applied Physics Letters, 2003. **83**(23): p. 4821-4823.
29. Lee, J.-H., et al., *Density-controlled growth and field emission property of aligned ZnO nanorod arrays.* Applied Physics A, 2009. **97**(2): p. 403-408.
30. Banerjee, D., S.H. Jo, and Z.F. Ren, *Enhanced Field Emission of ZnO Nanowires.* Advanced Materials, 2004. **16**(22): p. 2028-2032.
31. Berdinsky, A.S., et al., *Field enhancement factor for an array of MWNTs in CNT paste.* Applied Physics A, 2006. **83**(3): p. 377-383.
32. Wang, W.Z., et al., *Aligned Ultralong ZnO Nanobelts and Their Enhanced Field Emission.* Advanced Materials, 2006. **18**(24): p. 3275-3278.